GOALS: The Great Observatories All-sky LIRG Survey
Third Data Delivery (Final)
8 April 2011

1. Introduction

This document describes the final data delivery of the Spitzer Legacy program, GOALS. The Great Observatories All-sky LIRG Survey (GOALS) combines new and archival imaging and spectroscopic data from NASA's Spitzer, Hubble, Chandra and GALEX observatories in a comprehensive survey of 202 of the most luminous infrared-selected galaxies in the local Universe (Armus et al. 2009). This delivery contains Spitzer imaging (IRAC and MIPS) and spectroscopic (IRS) data for 121 nuclei in 98 systems in the GOALS sample. This document is organized as follows: section 2 lists the data products, their general characteristics and naming convention, and sections 3, 4, and 5 provide a description of the post-BCD processing for IRAC, MIPS and IRS data, respectively.

2. Content of the data delivery

The 102 galaxies included in this second delivery were selected from the complete GOALS sample. Table 1 lists the galaxies with images and spectra in this delivery. The following is a list of data products:

- IRAC image mosaics at 3.6, 4.5, 5.6 and 8μm. All images are single-extension FITS files. The pixel scale of the mosaics are 0.6 arcsec, and the flux (surface brightness) units are MJy/sr. The mosaics have standard orientation with North up and East to the left.
- MIPS image mosaics at 24, 70, and 160 microns. All images are single-extension FITS files. The pixel scale of the mosaics are wavelength dependent: 1.8 arcsec at 24μm, 4.0 arcsec at 70μm, and 8.0 arcsec at 160μm. The flux (surface brightness) units in all cases are MJy/sr. The mosaics have standard orientation with North up and East to the left.
- IRS nuclear spectra in the Short-Low, Long-Low, Short-High and Long-High modules. IRS spectra are delivered in ASCII (*.tbl) format, similar to those produced by the IRS pipeline. The flux units are Jy. An example spectrum is shown in Figure 1.

2.1 File Naming Convention

For each galaxy, the delivered Spitzer data have the following filename conventions:

- **IRAC mosaics**: NAME_irac_chN.fits, where NAME is the object name and N is the channel number (1 = 3.6 μm, 2 = 4.5 μm, 3 = 5.8 μm, and 4 = 8 μm)
- **MIPS mosaics**: NAME_mips_chN.fits, where NAME is the object name and N is the channel number (1 = 24 μm, 2 = 70 μm, and 3 = 160 μm)
- **IRS spectra**: NAME_chN.tbl, where NAME is the object name and N is the channel number (0 = SL, 1 = SH, 2 = LL, 3 = LH).

Table 1: GOALS Sources

NGC0034	11.44	00h11m06.55s	-12d06m26.3s
ESO350-IG038	11.22	00h36m52.50s	-33d33m19.0s
IC1623AB	11.65	01h07m47.18s	-17d30m25.3s
MCG-03-04-014	11.63	01h10m08.96s	-16d51m09.8s
CGCG436-030	11.63	01h20m02.72s	+14d21m42.9s
ESO297-G011	11.09	01h36m23.78s	-37d19m51.9s
IRASF01364-1042	11.76	01h38m52.92s	-10d27m11.4s
IRASF01417+1651	11.56	01h44m30.50s	+17d06m05.0s
NGC0695	11.63	01h51m14.24s	+22d34m56.5s
NGC0828	11.31	02h10m09.57s	+39d11m25.3s
MCG+05-06-036	11.59	02h23m20.45s	+32d11m34.2s
NGC0958	11.17	02h30m42.58s	-02d56m27.2s
NGC1068	11.27	02h42m40.71s	-00d00m47.8s
UGC02238	11.26	02h46m17.49s	+13d05m44.4s
IRASF02437+2122	11.11	02h46m39.15s	+21d35m10.3s
NGC1275	11.2	03h19m48.16s	+41d30m42.1s
NGC1365	11	03h33m36.37s	-36d08m25.4s
IRASF03359+1523	11.47	03h38m46.70s	+15d32m55.0s
UGC02982	11.13	04h12m22.45s	+05d32m50.6s
ESO550-IG025	11.45	04h21m20.00s	-18d48m48.0s
NGC1572	11.24	04h22m42.81s	-40d36m03.3s
NGC1614	11.6	04h33m59.85s	-08d34m44.0s
UGC03094	11.35	04h35m33.83s	+19d10m18.2s
ESO203-IG001	11.79	04h46m49.50s	-48d33m32.9s
VIIZw031	11.94	05h16m46.44s	+79d40m12.6s
IRASF05187-1017	11.23	05h21m06.54s	-10d14m46.7s
IRAS05223+1908	11.59	05h25m16.50s	+19d10m46.0s
NGC1961	11.02	05h42m04.80s	+69d22m43.3s
ESO255-IG007	11.84	06h27m23.10s	-47d10m47.0s
ESO557-G002	11.19	06h31m47.22s	-17d37m17.3s
IRASF07027-6011	11.58	07h03m24.12s	-60d15m23.3s
NGC2342	11.25	07h09m18.08s	+20d38m09.5s
NGC2369	11.1	07h16m37.73s	-62d20m37.4s
NGC2388	11.23	07h28m53.44s	+33d49m08.7s
MCG+02-20-003	11.08	07h35m43.37s	+11d42m33.5s
ESO60-IG16	11.76	08h52m29.90s	-69d01m58.0s
UGC04881	11.69	09h15m55.10s	+44d19m55.0s
MCG+08-18-013	11.28	09h36m37.19s	+48d28m27.7s
IRASF09437+0317	11.19	09h46m20.60s	+03d03m30.0s

NGC3110	11.31	10h04m02.11s	-06d28m29.2s
IRASF10038-3338	11.73	10h06m04.80s	-33d53m15.0s
IRASF10173+0828	11.8	10h20m00.22s	+08d13m34.0s
NGC3256	11.56	10h27m51.27s	-43d54m13.8s
ESO264-G057	11.08	10h59m01.79s	-43d26m25.7s
MCG+07-23-019	11.61	11h03m53.20s	+40d50m57.0s
CGCG011-076	11.37	11h21m12.26s	-02d59m03.5s
IC2810	11.59	11h25m45.05s	+14d40m35.9s
NGC 3690	11.88	11h28m32.20s	+58d33m44.0s
ESO320-G030	11.1	11h53m11.72s	-39d07m48.9s
IRASF12224-0624	11.27	12h25m03.91s	-06d40m52.6s
NGC4418	11.08	12h26m54.62s	-00d52m39.2s
NGC4922	11.32	13h01m24.90s	+29d18m40.0s
CGCG043-099	11.62	13h01m50.80s	+04d20m00.0s
MCG-02-33-098	11.11	13h02m19.70s	-15d46m03.0s
IC 0860	11.17	13h15m03.53s	+24d37m07.9s
VV250a	11.74	13h15m35.02s	+62d07m28.8s
UGC08387	11.67	13h20m35.34s	+34d08m22.2s
NGC5104	11.2	13h21m23.08s	+00d20m32.7s
NGC5135	11.17	13h25m44.06s	-29d50m01.2s
NGC5256	11.49	13h38m17.50s	+48d16m37.0s
NGC5257	11.55	13h39m55.20s	+00d50m13.0s
UGC08739	11.08	13h49m13.93s	+35d15m26.8s
ESO221-IG010	11.17	13h50m56.94s	-49d03m19.5s
NGC5331	11.59	13h52m16.20s	+02d06m16.0s
NGC5394	11	13h58m35.80s	+37d26m20.0s
IC4518AB	11.13	14h57m42.90s	-43d07m54.0s
CGCG049-057	11.27	15h13m13.10s	+07d13m31.8s
VV705	11.89	15h18m06.34s	+42d44m36.7s
ESO099-G004	11.67	15h24m58.19s	-63d07m34.2s
NGC6052	11.02	16h05m12.90s	+20d32m32.0s
IRASF16164-0746	11.55	16h19m11.79s	-07d54m02.8s
CGCG052-037	11.38	16h30m56.54s	+04d04m58.4s
IRASF16399-0937	11.56	16h42m40.21s	-09d43m14.4s
NGC6240	11.85	16h52m58.89s	+02d24m03.4s
IRASF16516-0948	11.24	16h54m24.03s	-09d53m20.9s
NGC6286	11.32	16h58m31.38s	+58d56m10.5s
IRASF17138-1017	11.42	17h16m35.60s	-10d20m38.0s
IRASF17207-0014	12.39	17h23m21.93s	-00d17m00.4s
NGC6621	11.23	18h12m55.31s	+68d21m48.4s
IC4687	11.55	18h13m39.63s	-57d43m31.3s
CGCG142-034	11.11	18h16m40.66s	+22d06m46.1s
NGC6670AB	11.6	18h33m35.15s	+59d53m21.0s
NGC6786	11.43	19h10m59.10s	+73d25m06.0s
ESO593-IG008	11.87	19h14m30.90s	-21d19m07.0s
IRAS19542+1110	12.04	19h56m35.44s	+11d19m02.6s
ESO339-G011	11.12	19h57m37.54s	-37d56m08.4s
NGC6926	11.26	20h33m06.11s	-02d01m39.0s
IRAS20351+2521	11.54	20h37m17.72s	+25d31m37.7s

ESO343-IG013	11.07	21h36m11.00s	-38d32m37.0s
NGC7130	11.35	21h48m19.50s	-34d57m04.7
IC5179	11.16	22h16m09.10s	-36d50m37.4s
ESO602-G025	11.27	22h31m25.48s	-19d02m04.1s
NGC7469	11.59	23h03m15.62s	+08d52m26.4s
CGCG453-062	11.31	23h04m56.53s	+19d33m08.0s
NGC7592	11.33	23h18m22.54s	-04d24m58.5s
ESO077-IG014	11.7	23h21m04.30s	-69d12m54.0s
NGC7674	11.5	23h27m56.72s	+08d46m44.5s
MCG-01-60-022	11.21	23h41m54.10s	-03d38m29.0s
NGC7752	11.01	23h47m01.63s	+29d28m17.2s
Mrk331	11.41	23h51m26.80s	+20d35m09.9s

Table 1. GOALS sources included in this delivery: Object name is given in Col.1, infrared luminosity (log L_{IR} in units of $L_{\odot}$) is given in Col.2, and RA and DEC (J2000) are given in Cols. 3 & 4, respectively. For multiple sources (e.g., merging pairs) only one entry is given for the system, with the position and luminosity corresponding to those derived from the original IRAS data.

3. IRAC Data Processing

Initial steps of the IRAC data reduction were provided by Version S11 of the Spitzer Science Center (SSC) pipeline. Further processing was performed using a combination of IDL and IRAF routines. Detector artifacts in the IRAC data include "banding," "muxbleed," and "column pulldown," as described in the IRAC Data Handbook (2006). Several steps were taken to improve upon the Basic Calibrated Data (BCD) from the SSC pipeline. First, instrumental artifacts were removed. The 3.6 and 4.5 μm images suffer from muxbleed and pulldown affecting the rows and columns (respectively) that contain cosmic ray hits, bright stars, or bright galactic nuclei. The 5.8 and 8.0μm images often have banding artifacts extending along the rows containing galactic nuclei or other bright features. IDL routines developed by the IRAC Instrument Support Team were used to correct all three types of artifact. However, residuals from these correction techniques remain in the final images, especially residual banding at 8μm. The first frame of the 5.8μm data was always excluded due to excessively high background levels compared to the other frames. For each field containing the target galaxy or interacting system, individual BCD images were spatially aligned, resampled, and combined into a mosaic image. The SSC Post-BCD software package MOPEX was used for the alignment and resampling, and to mask out known bad pixels in each band. The IRAF module imcombine was used to make mosaics using the images output by MOPEX. Cosmic ray artifacts were removed by sigma-clipping when the mosaics were constructed. In some cases, most often in the 5.8μm mosaics, background mismatches between BCD images were corrected using the overlap script within the MOPEX package. Although overlap effectively removes background variations between adjacent images, large-scale gradients over a mosaic are preserved. The overlap routine also provides an alternative means of cosmic ray removal.

Due to the presence of bright galactic nuclei, we utilized the high dynamic range (HDR) mode in all four bands. The HDR frames are comprised of 1-2 sec exposures ("short" integration) to calibrate pixels that would have saturated in the 30-second exposures ("long" integrations). Data presented here are mosaics of the long integrations where such mosaics are not saturated. In the event of saturation (very rare for ch1-3, common for ch4), short exposure mosaics are used instead. The EXPTIME header keyword indicates which type of mosaic has been provided.

For each mosaic, the background level has been measured and subtracted from the image. This value is recorded in the BACKGROU header keyword.

3.1 *Notes on Individual Objects*

NGC7552 was delivered by SINGS and can be found at
http://irsa.ipac.caltech.edu/data/SPITZER/SINGS/galaxies/ngc7552.html

The IRAC channel 3 (5.8 μm) mosaic of UGC08739 suffers from extreme cosmic ray contamination due to the solar storm of mid-January 2005, and is not included in the GOALS delivery.

4. MIPS Data Processing

4.1. *The 24 μm Si:As Detector Array*

The BCD pipeline products from the 24 μm channel of MIPS contain some artifacts, mostly due to very bright flux densities, for many of the sources in our program (see Table 2). Notable features in the Si:As (IBC) array data are bright latent image spots trailing along the in-scan direction from bright sources (very rare), and in some cases dark latents (1-2% depressions in responsivity) for sources brighter than about 18 Jy. Residual gradients in the background from the pipeline flat-fielding process are also present at the 1-2% level in many of the 24 μm images. A weak "jail-bars" effect is often present in the BCDs, reflecting different readout gains rather than saturation. Another potential problem is optical distortion at 24 μm, which can induce photometric calibration variations of 2-10% across the array in some frames; the post-BCD pipeline reductions correct for this particular problem using MOPEX. More detailed descriptions and illustrations of these instrumental effects are given in the MIPS Data Handbook (2006). Where possible, the self-calibration procedure (self-cal) was used to remove latents and weak jailbars. However, often the small number of input images (14, for the most common AOR) precluded self-calibration. The overlap routine discussed in §3, which is part of the MOPEX package, was used in the initial stages of mosaic creation at 24μm. The final mosaics, after treatment for saturation effects where present (§§4.3), were constructed using the mosaic routine of MOPEX.

4.2. *The 70 and 160μm Ge:Ga Detector Arrays*

MOPEX was used to resample and align the MIPS BCD images and combine them while rejecting pixels flagged as suffering from latent image artifacts. The 70μm BCD images were filtered using column filter and time filter IDL routines created by D. Fadda. These routines offer an improvement over the filtered BCD images generated by the pipeline by masking the position of the target(s) prior to filtering. MOPEX was used to align, resample, and combine the filtered MIPS images into final mosaics in all three MIPS bands.

For each mosaic (ch1-3), the background level has been measured and subtracted from the image. This value is recorded in the BACKGROU header keyword. Note that the filtering procedure used on the ch2 data removes most of the background, resulting in the very small, sometimes negative BACKGROU values recorded for those mosaics. The ν^{-2} color corrections from the MIPS Data Handbook have been applied to the flux densities listed in Table 2.

4.3. *Treatment of MIPS Saturation Problems*

The bright galactic nuclei in our sample presented saturation problems for many of the MIPS observations. The saturation limits for a 1-second observation of a point source are approximately 4 Jy, 18 Jy, and 3 Jy at 24, 70, and 160μm, respectively. At 24μm, a strong "jailbar" pattern with depressed responsivity in every fourth column appears around saturated sources; bright 24μm sources may also saturate parts of the array, resulting in a DC offset that thwarts the pipeline's default "droop correction" algorithm. Individual frames displaying these saturation problems were removed prior to the creation of the final mosaic with MOPEX using the remaining frames that did not display indications of saturation. The typical pattern in the data was several saturated images (strong "jailbar" pattern) followed by useful, unsaturated data frames.

At 70 and 160μm, the Spitzer MIPS Ge Reprocessing Tools (GeRT) package was utilized to correct the BCDs for saturation problems. To fix saturated pixels, the GeRT mosaic was matched to the initial MOPEX mosaic by computing their ratio and scaling the GeRT mosaic appropriately. A pixel mask was then applied, and the missing pixel(s) from the GeRT mosaic were used to produce a corrected MOPEX mosaic. The GeRT was configured to require a minimum of two data samples to estimate the slope of the signal. Severely saturated images, which are saturated on the first or second point of the integration ramp, could not be recovered with the GeRT, and are thus unusable for photometry.

4.3.1 *Notes on Individual Objects*

NGC7552 was delivered by SINGS and can be found at
http://irsa.ipac.caltech.edu/data/SPITZER/SINGS/galaxies/ngc7552.html

MCG+20-02-003 and VV250a were not observed by MIPS.
NGC7130 was not observed in MIPS channel 3 (160μm).

Galaxies in this delivery with saturated MIPS channel 1 (24μm) data are: NGC1068. The central pixels of NGC3256 and NGC4418 appear to be marginally saturated. The eastern component of NGC3690 is saturated.
Galaxies in this delivery with saturated MIPS channel 2 (70μm) data are: IC1623AB.
Galaxies in this delivery with saturated MIPS channel 3 (160μm) data are: CGCG049-057, ESO320-G030, IC1623AB, IC5179, IRASF17207-0014, NGC0828, NGC1068, NGC1365, NGC2369, NGC3256, NGC3690, and NGC7469. NGC2388 is also saturated, but the companion galaxies are not and the mosaic is included in this delivery.

5. IRS Data Processing

For the low-resolution IRS spectra, off-source nods were used for sky subtraction, unless dedicated sky observations were available. For the high-resolution spectra, dedicated sky observations were used for subtraction where available. In all cases where dedicated sky observations were not available, nods were not subtracted due to the limited size of the LH and SH slits. In all cases for both high and low resolution spectra, one mask ("bmask") file was created per nod such that bmask_final[i,j]=max(bmask_N[i,j]) where i,j are the pixel coordinates and the bmask_Ns are the masks corresponding to each BCD containing the on-source spectrum, as well as each BCD used for sky subtraction. One uncertainty ("func") file was also created per nod by combining the func files associated with all applicable on- and off-source BCDs using standard propagation of error. On-source BCDs for each nod were combined using an average with 3-sigma clipping.

Each nod was extracted with SPICE using the standard extraction aperture, and point-source calibration. Nod-1 and nod-2 were compared with each other, with pixels flagged if the difference between nod1 and nod2 exceeded 10%, and when adjacent pixels within the same nod differed by >10% (i.e., from a cosmic ray or hot pixel). Flagged pixels were excluded when the nods were combined into the final spectrum for each object. In addition, the blue and red ends of all spectral orders have been trimmed to remove noisy or poorly calibrated data. Typically 5 pixels were removed from the blue end and 10-20 pixels were removed from the red end of the SH and LH data, while 2-3 pixels are removed from the ends of the SL and LL data. The resulting wavelength coverage is 5 – 36μm in low-res and 19 – 37μm in high-res. A sample spectrum of NGC6701 is shown in Fig. 1.

5.1 Notes on individual objects and data features

Order mis-matches (tilts) are sometimes seen in the IRS LH data. These are inherent in some of the pipeline products from the SSC, and we have decided not to adjust the spectra to remove them, since they do not, in most cases, affect the derived line fluxes. Continuum slopes for the LIRGs in GOALS are best determined from the SL and LL data. In particular, LH mismatches are seen in the following objects: IRASF01417+1651, NGC1068, ESO203-IG001, IRAS05223+1908, NGC4418, VV705, IRASF16399-0937, IRASF17207-0014, and IRAS19542+1110.

Spectral fringing is visible in the IRS LL 1st order spectra of the following objects: ESO255-IG007_3, NGC1614, and NGC7130.

Two sources are resolved in the SL slit for NGC5256 (the northern source NGC5256 and the southern source NGC5256_2) but only one source (the southern source NGC5256_2) falls in the LL slit. Both an SL and an LL spectrum are thus provided for NGC5256_2, but only an SL spectrum is available for NGC5256.

Five objects were not observed with the IRS: ESO550-IG025, IC4518AB, MCG+08-18-013 (no SL only; LL & high-res provided), NGC2388 (no LL only; SL & high-res provided), and VV705 (no LL only; SL & high-res provided for the southern source). NGC1068 was observed, but saturates the low-res detector and no low-res spectrum is provided (see Howell et al. 2007 for details). For three objects either the SL (IRASF03359+1523; MCG-01-60-022) or LL (NGC4922) slit was not centered on the galaxy nucleus, and these spectra are not provided in this delivery. For the high-res observations the following spectra are not provided due to their off-nucleus slit positions: IRASF01417+1651(no SH only; LH provided), NGC5257 (no high-res). Note that there are four pointings whose slits only cover about half of the galaxy nuclei: NGC1614, NGC5135, IRASF17138-1017, and NGC7130.

Although the vast majority of GOALS IRS spectra are derived from IRS Staring Mode data, some of the archival GOALS data were taken only in IRS Mapping mode. For these sources, in order to have a direct comparison with the dominant Staring Mode nuclear spectra, we have extracted "pseudo staring mode" spectra from the spectral maps using CUBISM (Smith et al. 2007). These galaxies are: NGC0034, IC1623, NGC2369, NGC3110, CGCG011-076, NGC3690, ESO320-G030, CGCG049-057, NGC6052, IRASF17138-1017 (LL only), NGC6621, IC4687, IC5179, NGC7592, and NGC7674). In all cases a two-step process was applied. First, 2x5 pixel extraction apertures centered on the galaxy's nucleus were used to extract nuclear spectra from the spectral cubes, and then a mapping-to-staring-mode correction (a multiplicative factor that is a smoothly varying function of wavelength derived from comparing mapping and staring mode observations of NGC6240 and a number of standard stars), was applied to each nuclear spectrum to create the "pseudo staring mode" spectrum. The correction was necessary because spectra that are extracted from IRS Mapping Mode data with CUBISM use calibration files which assume a flat distribution across the slit for flux calibration (aperture and slit loss corrections), and these are not the same as used in the pipeline (or with SPICE) for Staring Mode data (which apply a point source calibration by default). The typical correction factor is 1.8 across SL and 1.9 across LL.

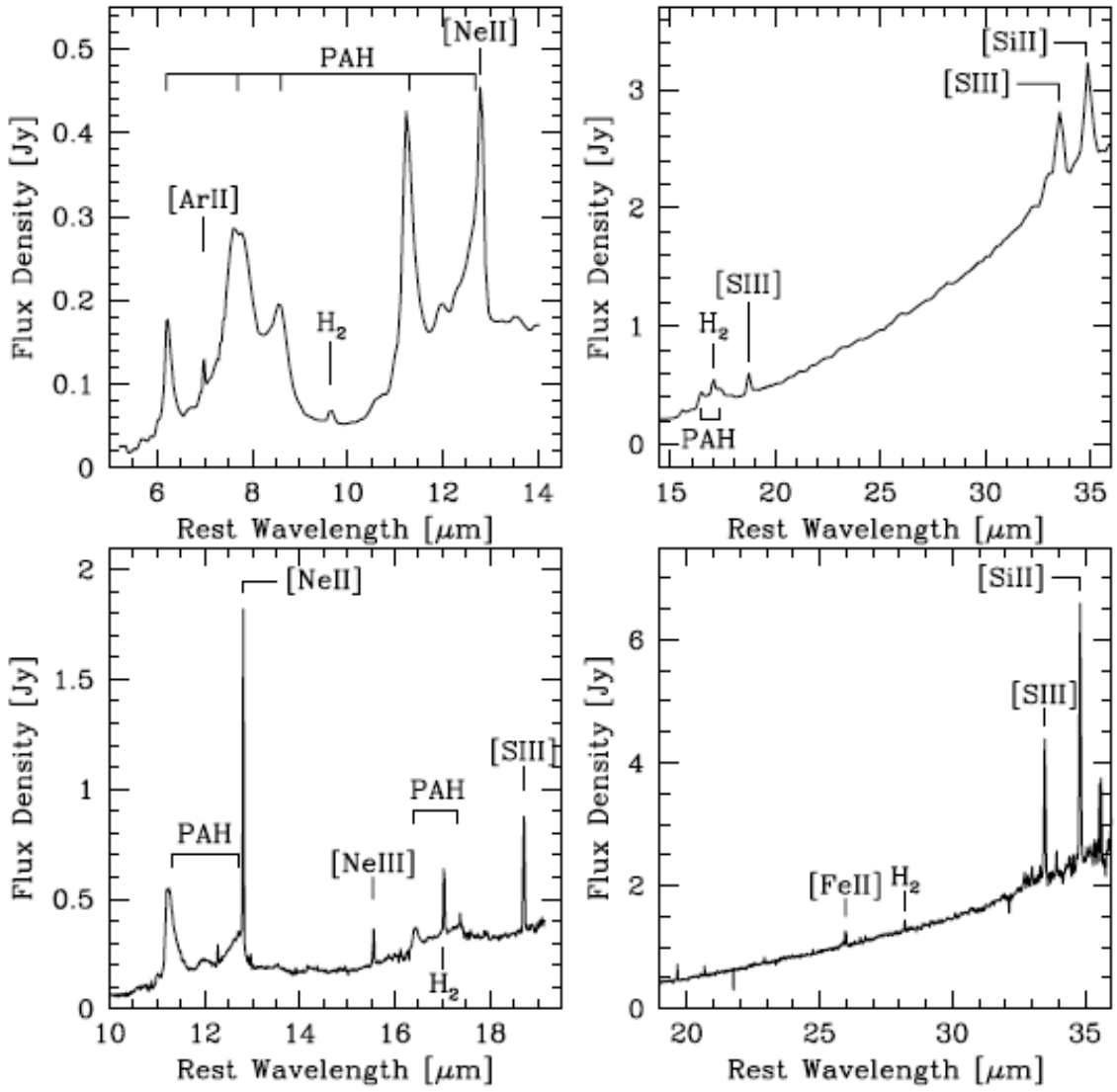

Fig. 1: IRS spectra of NGC6701 (from the first GOALS delivery). Short-low is in the top left panel, long-low in the top right, short-high in the bottom left, and long-high in the bottom right.

References

Armus, L., et al. 2009, PASP, 121, 559.

Howell, J.H., et al. 2007, AJ, 134, 2086.

Smith, J.D.T., et al. 2007, PASP, 119, 1133.